Trans-membrane association of the Sec and BAM complexes for bacterial outer-membrane biogenesis

Sara Alvira[1*], Daniel W. Watkins[1*], Lucy Troman[1], James Lorriman[1], Bertram Daum[2], Vicki A.M. Gold[2] and Ian Collinson[1†]

[1], *School of Biochemistry, University of Bristol, BS8 1TD, United Kingdom*

[2], *Living Systems Institute, Stocker Road, Exeter, Devon EX4 4QD, United Kingdom*

[*], these authors contributed equally to this work

[†], corresponding author: ian.collinson@bristol.ac.uk

ABSTRACT

The outer-membrane of Gram-negative bacteria is critical for surface adhesion, pathogenicity, antibiotic resistance and survival. The major constituents –hydrophobic β-barrel Outer-Membrane Proteins (OMPs)– first need to secreted across the inner-membrane by the Sec-translocon. Following their emergence from the protein-channel in the periplasm, chaperones such as SurA and Skp pick up the cargo to prevent aggregation. The chaperoned OMPs are somehow then delivery through the Peptido-Glycan layer (PG) to the β-Barrel Assembly Machinery (BAM), where insertion and folding into the outer-membrane occurs. It is very unclear how vast quantities of protein, required for rapid cell wall biogenesis, are trafficked to the outer-membrane while avoiding aggregation, and in the absence of energy. Here, we present *in vitro* and *in vivo* biochemical analyses, supported by electron microscopy, to show the Holo-TransLocon (HTL; a complex of the core-translocon SecYEG with the accessory proteins SecDF-YajC, and the membrane protein 'insertase' YidC) contacts the periplasmic chaperone SurA, and BAM of the outer-membrane. The interaction bestows a new role for the ancillary sub-complex SecDF, which contacts BAM *via* their extended periplasmic domains. The connection provides a contiguous pathway between the inner- and outer-membrane; for safe and efficient passage of unfolded β-barrel proteins directly to the surface. This inter-membrane conduit would prevent aggregation, and possibly even facilitate energy-transduction from the inner-membrane, conferred by SecDF, for outer-membrane protein insertion and folding. This interaction also provides specific new insight of trans-membrane organisation and communication; an area of increasing biological interest and significance.

INTRODUCTION

Outer-membrane biogenesis in Gram-negative bacteria (Konovalova et al., 2017) requires substantial quantities of protein to be transported, first of all, across the inner plasma membrane. Precursors of β-barrel Outer-Membrane Proteins (OMPs) with cleavable N-terminal signal-sequences are targeted to the ubiquitous Sec-machinery and driven into the periplasm by the ATPase SecA and the trans-membrane proton-motive-force (PMF) (Brundage et al., 1990; Lill et al., 1989); reviewed by (Collinson et al., 2015; Cranford-Smith and Huber, 2018). Upon completion the pre-protein signal-sequence is proteolytically cleaved (Chang et al., 1978; Josefsson and Randall, 1981), releasing the mature unfolded protein into the periplasm. The emergent protein is then picked up by periplasmic chaperones, such as SurA and Skp that prevent aggregation (McMorran et al., 2013; Sklar et al., 2007), and somehow facilitate delivery to the β-Barrel Assembly Machinery (BAM) for outer-membrane insertion and folding (Voulhoux et al., 2003; Wu et al., 2005).

In *E. coli* BAM consists of a membrane protein complex of subunits BamA-E, of known structure (Bakelar et al., 2016; Gu et al., 2016; Iadanza et al., 2016): it is composed of Bam A, a 16 stranded β-barrel integral membrane protein, that projects a large periplasmic stretch of 5 POlypeptide TRanslocation-Associated (POTRA) domains into the periplasm. BamB-E are peripheral membrane proteins that are anchored to the inner leaflet of the OM. In spite of the structural insights a mechanism for OMP insertion has not yet been described (Ricci and Silhavy, 2019).

The periplasm is a challenging environment for unfolded proteins, and complexes spanning both membranes are critical for efficient delivery through many specialised secretion systems (Green and Mecsas, 2016). So how do enormous quantities of proteins entering the periplasm *via* the general secretory pathway (Sec) efficiently find their way through the cell envelope to the outer-membrane? Could it be achieved by a direct interaction between chaperones, and the translocons, described above, of the inner- and outer-membranes?

The core-translocon, SecYEG, does not possess periplasmic domains of sufficient size to mediate such an interaction (Van den Berg et al., 2004). Interestingly, the Holo-TransLocon (HTL) contains the ancillary sub-complex SecDF and the membrane protein 'insertase' YidC (Duong and Wickner, 1997; Schulze et al., 2014); both of which contain periplasmic extensions potentially large enough to reach the POTRA domains of BamA. Our initial experiments

immediately showed that this was indeed the case. The basic properties of the trans-membrane complex were subsequently examined as well as its importance for OMP folding and insertion. The consequences of this interaction are profound; particularly for the mechanism of protein transport through the Sec and BAM complexes, and for outer-membrane biogenesis, which we discuss below.

RESULTS

Interaction between the Sec and BAM complexes

Experiments were conducted in which total *E. coli* membranes were fractionated by sucrose gradient centrifugation, to separate the inner- and outer-membranes. Membranes made from cells over-producing SecYEG by itself, showed that (as expected) the complex migrated with the inner membrane fractions. Whereas, SecYEG as part of HTL co-migrates more with the outer-membranes (Fig. 1a,b). This effect is maintained when SecDF is over-produced, but lost when the periplasmic domain of SecD (P1) is removed (Fig. 1c).

To further investigate this interaction, we extracted native membranes with a mild detergent, for ImmunoPrecipitation (IP) using a monoclonal antibody raised against SecG, and probed for native interactors by western blotting (Fig. 1d). As expected, SecG (positive control), SecY of the core Sec-complex, and SecD of HTL co-immuno-precipitated. Crucially, BamA could also be detected in these pull downs. The specificity of the association was demonstrated by controls omitting the SecG antibody or the SecG protein (produced from membranes extracts of a *ΔsecG* strain (Nishiyama et al., 1994)); wherein non-specific binding was either undetectable, or considerably lower than the specific co-immuno-precipitant (Fig. 1d; Fig. S1a). When BAM was over-produced, the yield of BamA recovered in the IPs increased accordingly (Fig. S1a). In a similar experiment, a hexa-histidine tag on recombinant over-produced BamA was used to isolate BAM, which co-purified with SecD and SecG of HTL (Fig. 1e). Again, controls (omitting Ni^{2+}) were reassuringly negative (Fig. S1b).

Requirement of the Sec-BAM interaction for cardiolipin

The phospholipid CardioLipin (CL) is known to be intimately associated with energy transducing systems, including the Sec-machinery –both for complex stabilisation and for efficient transport (Corey et al., 2018; Gold et al., 2010; Schulze et al., 2014). For this reason, the IP experiments above were augmented with CL; when it was omitted, the interactions of SecG with SecD and BamA were significantly reduced (Fig. 1f; Fig. S1c). This lipid enhanced SecG-SecD interaction is consistent with our previous finding that CL stabilises HTL (Schulze et al., 2014), and shows it is also true of the HTL-BAM interaction. *Apropos*, CL was recently shown to be associated with BAM (Chorev et al., 2018).

Isolation and analysis of the Sec-BAM complex

To confirm the interaction between the Sec and BAM machineries, the purified complexes were subject to glycerol gradient centrifugation. When mixed together, HTL and BAM co-migrated into fractions containing higher glycerol concentrations, beyond those attained by the individual complexes (Fig. 2a; Fig. S2a), consistent with an interaction between the two. When the experiment was repeated with the individual constituents of HTL, SecDF and YidC, but not SecYEG, were also shown to interact with BAM (Fig. S2b-d).

Visualisation of the heavy fractions containing interacting HTL and BAM by Negative Stain (NS)-Electron Microscopy (EM) revealed a highly heterogeneous mixture of small and very large complexes (Fig. S3a). This mixed population may be due to the expected transient nature of the interaction between the two complexes, or possibly super-complex instability caused by lipid (*e.g.* CL) extraction during purification (see below). To overcome this heterogeneity we stabilised the complex by cross-linking, using GraFix (Kastner et al., 2008)(Fig. 2a, right). Visualisation by NS-EM revealed a marked reduction in the number of dissociated complexes (Fig. S3b). As expected, omitting CL from the preparation resulted in dissociation of the majority of the large complexes (Fig. S3c).

Mass spectrometry confirmed the presence of BAM and HTL constituents in a high molecular weight GraFix fraction (Fig. 2a, asterisk; Table S1), selected for NS-EM. The subsequent single particle analysis of this material (Table S2) revealed a remarkable object with a 3D volume (~ 300 x 250 x 150 Å) large enough to contain both machineries (Botte et al., 2016; Iadanza et al., 2016), and with a height sufficient to straddle the space between the two membranes (Fig. 2b);

especially when considering the known flexibility of HTL and BAM, and the plasticity of the periplasm (Zuber et al., 2008).

To assign the locations and orientations of the individual constituents of HTL and BAM, we compared the 3D structures of different sub-complexes. BAM bound to SecYEG-DF (Fig. 2c) or SecDF alone (Fig. 2d), revealed the locations of YidC (Fig. 2c,d, pink arrow), SecDF and SecYEG (Fig. 2d, blue arrow) at the bottom of the assembly depicted in Figure 2f (assigned as the inner-membrane region). As predicted, YidC and SecDF seem to interact with BAM through their large periplasmic domains (Fig. 2f). The orientation of BAM and SecDF relative to one another is different in SecDF-BAM compared to HTL-BAM (Fig. 2d,f; Fig. S4), likely due to the absence of stabilising interactions with the rest of HTL components. The flexibility of the SecDF sub-assembly (in the absence of SecYEG) was also seen in the high-resolution structures (Furukawa et al., 2018; Tsukazaki et al., 2011). Removing BamB from the complex mainly affects the part of the assembly nearest the OM (Fig. 2e, orange arrow), confirming the assigned orientation shown in Fig. 2f. Interestingly, this complex seems to lack the density for YidC (Fig. 2e, pink arrow), suggesting that BamB is required to stably connect YidC.

The cardiolipin stabilised open holo-translocon associates with the BAM complex

An interesting feature of the HTL-BAM assembly is the larger more open appearance of the HTL, compared to the more compact low-resolution cryo-EM structure (Botte et al., 2016) (emd3056; Fig. S5a). The HTL preparation used here contained mostly the 'compact' form and a small proportion of the 'open' state. The 'open' state could be stabilised by CL and enriched by glycerol gradient centrifugation (Fig. S5b). Given the known requirement for CL for the stability and activity of the translocon (Brundage et al., 1990; Corey et al., 2018; Gold et al., 2010; Schulze et al., 2014), then the 'compact' state is most likely non-native. Moreover, the HTL contains an internal lipid core (Botte et al., 2016), which if depleted would cause the complex to collapse.

The lipid stabilised native-like 'open' structure, with proud periplasmic domains, presumably of SecDF and YidC, resembles the form associating with BAM (assembled in the presence of CL; Fig. S5a). The mixture of the 'open'-HTL and the lipid depleted 'compact'-HTL partly explains the observed heterogeneity of the assembled HTL-BAM sample (as noted above).

The HTL lipid core might be important for membrane protein insertion (Botte et al., 2016), and possibly also for preserving a viable trans-membrane conduit to the outer-membrane.

Interaction of the Sec machinery with SurA

Presumably, when proteins emerge in the periplasm from the Sec machinery they are quickly engaged by chaperones. Prime examples being Skp and SurA (McMorran et al., 2013; Sklar et al., 2007). So far, no evidence has been presented of a chaperone-Sec interaction. As noted above, the SecYEG core-complex, does not really contain periplasmic domains large enough to do so. So, again, we explored the possibility of such an interaction with the HTL, which once more proved successful (Fig. 3a; Fig. S6). The heterogeneity of the isolated HTL-SurA was similar to that of HTL-BAM, so samples for EM were again prepared by GraFix (Fig. 3a, right; Fig. S6a; Fig. S7a). NS-EM analysis revealed a structure with dimensions of roughly 300 x 250 x 150Å, large enough to contain both HTL and SurA (Fig. 3b). Analysis of immuno-decorated complexes by NS-EM, with a polyclonal antibody raised against SurA (Fig. 3c), or a monoclonal antibody specific to a cytosolic loop of SecY (Corey et al., 2016) (Fig. 3d), revealed the locations of these components and the orientation of the complex with respect to the inner-membrane.

The experiment was repeated using SurA purified in complex with a classical OMP substrate, OmpA (Fig. 3e,f; Fig. S6b; Fig. S7b). The NS-EM structure of HTL-SurA-OmpA shows additional density compared to HTL-SurA, roughly adjacent to the channel exit site of SecYEG and in contact with SurA, possibly representing a late inner-membrane translocation intermediate (Fig. 3f).

Some areas of chaperone associated HTL, and earlier HTL-BAM complexes, were somewhat larger than expected, compared to the X-ray structures; particularly in the transmembrane regions. This extra mass is presumably a result of the detergent micelle and extra lipids, which cannot be distinguished from protein at this resolution with NS (Thonghin et al., 2018; Vahedi-Faridi et al., 2013); the more open state of the HTL might also contribute to this increased size (discussed above).

Consequences of the Sec-BAM interaction

In light of these results, we reasoned that depleting essential components of BAM-HTL *in vivo* might specifically impair OMP biogenesis. To test this, we utilised the *E. coli* strain JP325, wherein the production of SecDF-YajC is under the control of an *ara* promoter: the presence of arabinose or glucose, respectively results in production or depletion of SecDF-YajC (Economou et al., 1995) (Fig. 4a). During depletion, the steady-state quantities of folded *versus* unfolded OmpA were monitored in the periplasm by SDS-PAGE and western blotting. This well-established assay distinguishes folded (fOmpA; Fig. 4b, lower band) and unfolded (ufOmpA; Fig. 4b, upper band) species of OmpA, and is a good test for OMP transport deficiencies (Bulieris et al., 2003; Sklar et al., 2007). The total amount of secreted OmpA (fOmpA + ufOmpA; Fig. 4b), adjusted for number of cells, was largely unaffected by SecDF-YajC depletion (Fig. 4c). Crucially though, depletion causes significant levels of the unfolded species to accumulate in the periplasm during the exponential phase of growth, when demand for OM biogenesis peaks (Fig. 4b, asterisk,d,e). This effect was not an indirect consequence of BamA loss, which was unperturbed (Fig. 4a). Presumably then, depletion of SecDF-YajC reduces the interaction opportunities of the Sec-machinery with BAM, hampering transport of β-barrel proteins to the outer-membrane and resulting in a build-up of ufOmpA in the periplasm. This would compromise the integrity of the outer-membrane and possibly explain the cold-sensitivity of *secD* mutants (Gardel et al., 1987).

DISCUSSION

Taken together, the *in vivo* and *in vitro* analyses point to the importance of the periplasmic domains of SecD, and possibly also YidC, for the functional interaction between the Sec and BAM translocons. The results even suggest a primary role SecDF for inter-membrane and trafficking and energy transduction –in keeping with other members of the RND transporter family, as in the AcrAB-TolC trans-membrane assembly (Du et al., 2014; Wang et al., 2017).

The resultant Sec-BAM super-complex highlights a new feature of trans-membrane organisation within the bacterial cell envelope, the importance of which is only just coming to the fore (Rassam et al., 2015; 2018). It remains to be determined exactly how this complex and the periplasmic chaperones coordinate. Perhaps the chaperones recognise emergent OMPs at the Sec-machinery and, together with SecDF, recruit BAM *via* the POTRA domains of BamA

(Fig. 4f). Other ancillary factors of the Sec machinery have also been implicated: YfgM and PpiD are thought to mediate interactions with periplasmic chaperones (Götzke et al., 2014). Interestingly, *yfgL* and *yfgM* are in the same operon (Blattner et al., 1997); the former of which encodes a subunit of BAM (BamB) (Wu et al., 2005).

Clearly the subsequent HTL-BAM interaction is required for efficient OMP biogenesis under cellular grown conditions. The interaction could enable large protein fluxes to stream through the periplasm, while minimising aggregation and proteolysis, required for massive quantities of OMP delivery to the cell surface (Fig. 4f). Moreover, the interaction is suggestive of the intriguing prospect of TonB-style energy-coupling from the inner membrane (Celia et al., 2016): *i.e.* the transmission of free energy available from ATP turnover and the PMF from the Sec-machinery (Arkowitz and Wickner, 1994; Brundage et al., 1990; Schiebel et al., 1991), for OMP folding and insertion at the outer-membrane.

Direct association between inner- and outer-membrane components appears to be the rule rather than the exception for transporters embedded in double membrane systems: parallels with the translocation assembly module (TAM) for auto-transporter secretion (Selkrig et al., 2012) and the TIC-TOC import machinery of chloroplasts (Chen et al., 2018) are particularly striking, given the respective outer-membrane components (TamA and TOC75) are homologous of BamA. More intriguing is the possibility of the mitochondrial homologue of BAM (Sorting and Assembly Machinery; SAM) participating in analogous trans-membrane interactions between respective inner- and outer-membranes. Indeed, subunits of the MItochondrial contact site and Cristae Organizing System (MICOS) connect the energy-transducing ATP synthase of the inner-membrane and SAM at the outer-membrane (Ott et al., 2015; Rampelt et al., 2017).

MATERIALS AND METHODS

Strains, plasmids and antibodies

E. coli C43 (DE3) was a gift from Sir John Walker (MRC Mitochondrial Biology Unit, Cambridge, UK) (Miroux and Walker, 1996). *E. coli* BL21 (DE3) was purchased as competent cells (New England Biolabs). *E. coli ΔsecG* (KN425 (W3110 M25 *ΔsecG*::kan)) (Nishiyama et al., 1994), which lacks a genomic copy of *secG*, was obtained from Prof. Frank Duong (University of British

Colombia, Vancouver, Canada). *E. coli* strain JP352 (Kan^r), which contains an arabinose-regulated *secDF-yajC* operon (Economou et al., 1995), was given to us by Prof. Ross Dalbey.

The plamids for over-expression of *secEYG* and *yidC* were from our laboratory collection (Collinson et al., 2001; Lotz et al., 2008), the former and also SecDF were acquired from Prof. Frank Duong (Duong and Wickner, 1997). HTL and HTL(ΔYidC) expression vectors were created using the ACEMBL expression system (Bieniossek et al., 2009; Botte et al., 2016). The vector for BAM over-expression pJH114 (Amp^r) was a gift from Prof. Harris Bernstein(Roman-Hernandez et al., 2014); from which pJH114-*bamACDE* (ΔBamB) was produced by linear PCR with primers designed to flank the BamB gene and amplify DNA around it. FseI restriction sites were included in the primers to ligate the amplified DNA. pBAD-SecDF(ΔP1) was generated by amplifying SecDF(ΔP1) from pBAD-SecDF and cloning it between the pBAD NcoI and HindIII sites. pET28b-*surA* and pET11a-*ompA*(Schiffrin et al., 2017) were a gifts from Prof. Sheena Radford (The Astbury Centre for Structural Molecular Biology, University of Leeds, UK).

All SDS-PAGE was performed with *Invitrogen* Bolt 4-12% Bis-Tris gels. For western blotting, proteins were transferred onto nitrocellulose membrane. Mouse monoclonal antibodies against SecY, SecE, SecG and YidC were from our laboratory collection. Polyclonal antibodies against SecD and BamA were generated commercially in rabbits, and SecA in sheep from purified proteins. BamB and BamD antibodies were gifts from Dr Harris Bertstein. The SurA antibody was purchased from 2BScientific. A secondary antibody conjugated to DyLight800 was used for SecG and SecY (Thermo Fisher Scientific), whereas the HRP-conjugated secondary antibody was used for SecD and BamA.

Protein expression and purification

HTL, HTL(ΔYidC), SecYEG, YidC, SecDF and SurA were purified as described previously (Burmann et al., 2013; Collinson et al., 2001; Lotz et al., 2008; Schulze et al., 2014). BAM and BAM(ΔBamB) was over-produced in *E. coli* C43 and purified as described previously (Iadanza et al., 2016; Roman-Hernandez et al., 2014). For preparation of SurA and SurA-OmpA complexes, both proteins were over-produced separately in 1 L of cultures as described previously(Humes et al., 2019). Both were harvested by centrifugation, lysed in a cell disruptor (Constant Systems Ltd.) and resuspended in 20 mL 20 mM Tris pH 8.0, 130 mM NaCl, 10 % (v/v) glycerol ($TS_{130}G$) in the presence of cOmplete protein inhibitor cocktail (Roche). The resulting

samples were clarified by centrifugation in an SS34 rotor (27,000 *g*, 4°C, 20 minutes, Sorvall). For OmpA, the supernatant was discarded and the pellet resuspended in 20 mL $TS_{130}G$ + 6 M urea. The OmpA pellet was diluted to 80 mL with 6 M urea and mixed with the SurA supernant to give a final urea concentration of 4.8 M. The urea was removed by dialysing in 2 L $TS_{130}G$ for 6 hours at room temperature, then dialysing overnight at 4°C in 2 L fresh $TS_{130}G$. The sample was centrifuged under the same conditions as above and the supernatant loaded onto a 5 mL HisTrap HP column equilibrated with $TS_{50}G$. The column was washed with $TS_{50}G$ + 20 mM imidazole, and bound proteins eluted with $TS_{50}G$ + 300 mM imidazole. The eluents were loaded onto a HiTrap Q HP column equilibrated in $TS_{50}G$ and free SurA was found in the unbound fraction. A linear gradient of 0.05 - 1 M NaCl was applied over 60 mL and the fractions containing SurA-OmpA were taken for further analyses.

Isolation of inner and outer membranes

1 L of *E. coli* cultures expressing SecYEG or HTL were produced as described previously (Collinson et al., 2001; Komar et al., 2016; Schulze et al., 2014). The harvested cell pellets were resuspended in 20 mL $TS_{130}G$, homogenised with a potter, passed twice through a cell disruptor (Constant Systems Ltd.) for lysis and centrifuged to remove debris (SS34 rotor, Sorvall, 12,000 *g*, 20 minutes, 4°C). The supernatant was taken and layered upon 20 mL $TS_{130}G$ + 20 % (w/v) sucrose in a Ti45 tube and centrifuged (Ti45 rotor, Beckmann-Coulter, 167,000 *g*, 120 minutes, 4°C). The pellet was taken, resuspended in 4 mL $TS_{130}G$, homogenised with a potter and layered upon a sucrose gradient prepared in an SW32 centrifuge tube composed of 5 mL layers of $TS_{130}G$ + 55 % (w/v), 48 % (w/v), 41 % (w/v), 34 % (w/v) and 28 % (w/v) sucrose. The sample was then purified by centrifugation (SW32 rotor, Beckmann-Coulter, 130,000 *g*, 15 hours, 4°C). On completion, the sample was fractionated and the resulting samples were analysed by SDS PAGE and western blotting.

Co-immunoprecipitations (co-IPs) with *E. coli* total membrane extracts

Membrane pellets of *E. coli* strains BL21 (WT), BL21 pJH114-*bamABCDE* (Amp^r) and *ΔsecG* (Kan^r) were prepared as described previously (Collinson et al., 2001), with *bamABCDE* over-expression also conducted as described previously(Roman-Hernandez et al., 2014). The pellets were resuspended in $TS_{130}G$ to 120 mg/mL, homogenised and solubilised with either 0.5% DDM

or 0.5 % (w/v) DDM supplemented with 0.05 % (w/v) CL for 1 hour at 4 °C. The solubilised material was clarified by ultra-centrifugation (160,000 *g* for 45 mins) and the membrane extracts were taken for analysis.

For co-IPs pulling on SecG antibody, 250 uL of protein G resin was washed in a spin column with 200 mM NaCl, 20 mM HEPES pH 8.0 (HS buffer), which was supplemented with either 0.02 % (w/v) DDM or 0.02 % (w/v) DDM / 0.002 % (w/v) CL, and blocked overnight in HS buffer + 2 % (w/v) BSA at 4°C. Meanwhile, 7.5 µL of SecG purified monoclonal antibody was added to 500 µL of the membrane extracts and incubated overnight at 4 °C. The following morning, the resin was washed thoroughly in HS buffer, resuspended back to 250 µL and added to the 500 µL of membrane extract for three hours at room temperature. The resin was separated from the extracts by centrifugation in a spin column at 3,000 *g* for 2 minutes, washed 8 times with 350 µL HS buffer, the last wash being collected for analysis, then the bound material was eluted by addition of 1 x LDS sample buffer. Samples were analysed by SDS PAGE and western blotting.

For co-affinity adsorption by pulling on the hexa-histidine tag of recombinant BamA, 100 µL of nickel-charged chelating resin was added to 500 µL of membrane extracts and incubated for 5 minutes at room temperature. The resin was then separated from the extract and treated in the same way as described above but with $TS_{130}G$ + 0.02 % (w/v) DDM/ 0.002 % (w/v) CL + 30 mM imidazole (washing) or 300 mM imidazole (elution).

In vitro assembly and purification of complexes for EM

All protein complexes visualized by EM were formed by incubating 5 µM of the respective proteins in binding buffer (20 mM HEPES pH 8.0, 250 mM NaCl, 0.03 % (w/v) DDM/ 0.003 % (w/v) CL at 30 ºC for 30 minutes with shaking in a total volume of 150 µl. The protein complexes were purified in a glycerol/ glutaraldehyde gradient (20 - 40 % (w/v) and 0 - 0.15 % (w/v), respectively) by centrifugation at 34,000 RPM in a SW60 Ti rotor (Beckmann-Coulter) for 16 hours at 4 ºC. Mobility controls of individual and partial complexes (BAM, BAM(ΔBamB), HTL, HTL(ΔYidC) or individual proteins (SecYEG, YidC, SecDF, SurA) without the glutaraldehyde gradient were performed under the same conditions. Gradients were fractionated in 150 µl aliquots and those with glutaraldehyde were inactivated with 50 mM of Tris pH 8.0. Aliquots were analysed by SDS-PAGE and silver staining.

EM and image processing

Aliquots of sucrose gradient fractions containing the different complexes were applied to glow-discharged (15 s) carbon grids with Cu 300 mesh, washed and stained with 2 % (w/v) uranyl acetate (1 min). Digital images were acquired with two different microscopes; a Tecnai 12 with a Ceta 16M camera (ThermoFisher Scientific at a digital magnification of 49,000 and a sampling resolution of 2.04 Å per pixel, and in a Tecnai 12 with a Gatan Camera One View at a digital magnification of 59,400 and a sampling resolution of 2.1 Å per pixel. Image processing was performed using the EM software framework Scipion v1.2(la Rosa-Trevín et al., 2016). Several thousand particles were manually selected as input for automatic particle picking through the XMIPP3 package(Abrishami et al., 2013; la Rosa-Trevín et al., 2013). Particles were then extracted with the Relion v2.1 package(Kimanius et al., 2016; Scheres, 2012a) and classified with a free-pattern maximum-likelihood method (Relion 2D-classification). After manually removing low quality 2D classes, a second round of 2D classification was performed with Relion and XMIPP-CL2D in parallel (Sorzano et al., 2010). Representative 2D averages were used to generate several initial 3D models with the EMAN v2.12 software(Scheres, 2012b; Tang et al., 2007). Extensive rounds of 3D classification were then carried out using Relion 3D-classification due to the heterogeneity of the sample. The most consistent models were used for subsequent 3D classifications. For the final 3D volume refinement, Relion auto-refine or XMIPP3-Projection Matching was used. Resolution was estimated with Fourier shell correlation using 0.143 correlation coefficient criteria(Rosenthal and Henderson, 2003; Scheres and Chen, 2012). Docking of the available X-ray atomic structures into the 3D reconstructions was performed manually using USCF Chimera(Pettersen et al., 2004). See Table S2 for image processing details.

Depletion of SecDF-YajC

A preculture of *E. coli* strain JP352 was prepared in 100 mL 2xYT media supplemented with 0.2 % (w/v) arabinose. The following morning, the cells were harvested by centrifugation and resuspended with fresh 100 mL 2xYT (no arabinose), 20 mL of which was used to inoculate a 2 L 2xYT culture containing either 0.2 % (w/v) arabinose or 0.5 % (w/v) glucose. An aliquot was taken every hour for approximately 6 hours. Periplasmic and outer membrane fractions were produced by preparing spheroplasts(Birdsell and Cota-Robles, 1967), centrifugating the samples at 4,000 *g* for 5 minutes, taking the supernatant (mixture of periplasmic and OM fractions) and removing the

OM fraction by ultracentrifugation at 130,000 *g* for 30 minutes. The fractions were subjected to SDS PAGE and western blotting.

Acknowledgments: We thank Dr William Allen for critically reading the manuscript and many fruitful discussions. We are particularly grateful to the generosity of Dr Harris Bernstein for the kind gifts of the BamABCDE expression construct (pJH114) and antibodies, and Prof. Sheena Radford for SurA and OmpA expression plasmids. Thanks to Prof. Daniel Daley for telling us about YfgL and YfgM.

Funding: This work was funded by the BBSRC (BB/S008349/1 to IC, DWW and SA; BB/N015126/1 to IC and DWW; BB/M003604/1 to IC and SA; SWBioDTP – BB/J014400/1 and BB/J014400/1 to LT), EMBO (Long Term Fellowship – ALTF 710-2015, LTFCOFUND2013 and GA-2013-609409 – to SA) and the Elizabeth Blackwell Institute for Health Research, University of Bristol (Elizabeth Blackwell Bridging fellowship to SA).

Author contribution: SA, DWW, LT and IC designed and conducted experiments, assisted by JT; SA, DWW, LT and IC wrote the manuscript; VAMG and BD provided facilities and expertise, and edited the manuscript; IC, VAMG and BD secured funding; IC led the project.

Declaration: the authors declare no competing interests.

Data and materials availability: All data are available in the main text or the supplementary materials.

REFERENCES

Abrishami, V., Zaldívar-Peraza, A., la Rosa-Trevín, de, J.M., Vargas, J., Otón, J., Marabini, R., Shkolnisky, Y., Carazo, J.M., and Sorzano, C.O.S. (2013). A pattern matching approach to the automatic selection of particles from low-contrast electron micrographs. Bioinformatics *29*,

2460–2468.

Arkowitz, R.A., and Wickner, W. (1994). SecD and SecF are required for the proton electrochemical gradient stimulation of preprotein translocation. Embo J. *13*, 954–963.

Bakelar, J., Buchanan, S.K., and Noinaj, N. (2016). The structure of the β-barrel assembly machinery complex. Science *351*, 180–186.

Bieniossek, C., Nie, Y., Frey, D., Olieric, N., Schaffitzel, C., Collinson, I., Romier, C., Berger, P., Richmond, T.J., Steinmetz, M.O., et al. (2009). Automated unrestricted multigene recombineering for multiprotein complex production. Nat. Methods *6*, 447–450.

Birdsell, D.C., and Cota-Robles, E.H. (1967). Production and ultrastructure of lysozyme and ethylenediaminetetraacetate-lysozyme spheroplasts of Escherichia coli. J. Bacteriol. *93*, 427–437.

Blattner, F.R., Plunkett, G., Bloch, C.A., Perna, N.T., Burland, V., Riley, M., Collado-Vides, J., Glasner, J.D., Rode, C.K., Mayhew, G.F., et al. (1997). The complete genome sequence of Escherichia coli K-12. Science *277*, 1453–1462.

Botte, M., Zaccai, N.R., Nijeholt, J.L.À., Martin, R., Knoops, K., Papai, G., Zou, J., Deniaud, A., Karuppasamy, M., Jiang, Q., et al. (2016). A central cavity within the holo-translocon suggests a mechanism for membrane protein insertion. Sci Rep *6*, 38399.

Brundage, L., Hendrick, J.P., Schiebel, E., Driessen, A.J., and Wickner, W. (1990). The purified E. coli integral membrane protein SecY/E is sufficient for reconstitution of SecA-dependent precursor protein translocation. Cell *62*, 649–657.

Bulieris, P.V., Behrens, S., Holst, O., and Kleinschmidt, J.H. (2003). Folding and insertion of the outer membrane protein OmpA is assisted by the chaperone Skp and by lipopolysaccharide. J. Biol. Chem. *278*, 9092–9099.

Burmann, B.M., Wang, C., and Hiller, S. (2013). Conformation and dynamics of the periplasmic membrane-protein-chaperone complexes OmpX-Skp and tOmpA-Skp. Nat. Struct. Mol. Biol. *20*, 1265–1272.

Celia, H., Noinaj, N., Zakharov, S.D., Bordignon, E., Botos, I., Santamaria, M., Barnard, T.J., Cramer, W.A., Lloubes, R., and Buchanan, S.K. (2016). Structural insight into the role of the Ton complex in energy transduction. Nature *538*, 60–65.

Chang, C.N., Blobel, G., and Model, P. (1978). Detection of prokaryotic signal peptidase in an Escherichia coli membrane fraction: endoproteolytic cleavage of nascent f1 pre-coat protein. Proc. Natl. Acad. Sci. U.S.a. *75*, 361–365.

Chen, Y.-L., Chen, L.-J., Chu, C.-C., Huang, P.-K., Wen, J.-R., and Li, H.-M. (2018). TIC236 links the outer and inner membrane translocons of the chloroplast. Nature.

Chorev, D.S., Baker, L.A., Wu, D., Beilsten-Edmands, V., Rouse, S.L., Zeev-Ben-Mordehai, T.,

Jiko, C., Samsudin, F., Gerle, C., Khalid, S., et al. (2018). Protein assemblies ejected directly from native membranes yield complexes for mass spectrometry. Science *362*, 829–834.

Collinson, I., Breyton, C., Duong, F., Tziatzios, C., Schubert, D., Or, E., Rapoport, T., and Kühlbrandt, W. (2001). Projection structure and oligomeric properties of a bacterial core protein translocase. Embo J. *20*, 2462–2471.

Collinson, I., Corey, R.A., and Allen, W.J. (2015). Channel crossing: how are proteins shipped across the bacterial plasma membrane? Philos. Trans. R. Soc. Lond., B, Biol. Sci. *370*.

Corey, R.A., Allen, W.J., Komar, J., Masiulis, S., Menzies, S., Robson, A., and Collinson, I. (2016). Unlocking the Bacterial SecY Translocon. Structure *24*, 518–527.

Corey, R.A., Pyle, E., Allen, W.J., Watkins, D.W., Casiraghi, M., Miroux, B., Arechaga, I., Politis, A., and Collinson, I. (2018). Specific cardiolipin-SecY interactions are required for proton-motive force stimulation of protein secretion. Proc. Natl. Acad. Sci. U.S.a. *115*, 7967–7972.

Cranford-Smith, T., and Huber, D. (2018). The way is the goal: how SecA transports proteins across the cytoplasmic membrane in bacteria. FEMS Microbiol. Lett. *365*.

Du, D., Wang, Z., James, N.R., Voss, J.E., Klimont, E., Ohene-Agyei, T., Venter, H., Chiu, W., and Luisi, B.F. (2014). Structure of the AcrAB-TolC multidrug efflux pump. Nature *509*, 512–515.

Duong, F., and Wickner, W. (1997). Distinct catalytic roles of the SecYE, SecG and SecDFyajC subunits of preprotein translocase holoenzyme. Embo J. *16*, 2756–2768.

Economou, A., Pogliano, J.A., Beckwith, J., Oliver, D.B., and Wickner, W. (1995). SecA membrane cycling at SecYEG is driven by distinct ATP binding and hydrolysis events and is regulated by SecD and SecF. Cell *83*, 1171–1181.

Furukawa, A., Nakayama, S., Yoshikaie, K., Tanaka, Y., and Tsukazaki, T. (2018). Remote Coupled Drastic β-Barrel to β-Sheet Transition of the Protein Translocation Motor. Structure *26*, 485–489.e2.

Gardel, C., Benson, S., Hunt, J., Michaelis, S., and Beckwith, J. (1987). secD, a new gene involved in protein export in Escherichia coli. J. Bacteriol. *169*, 1286–1290.

Gold, V.A.M., Robson, A., Bao, H., Romantsov, T., Duong, F., and Collinson, I. (2010). The action of cardiolipin on the bacterial translocon. Proc. Natl. Acad. Sci. U.S.a. *107*, 10044–10049.

Götzke, H., Palombo, I., Muheim, C., Perrody, E., Genevaux, P., Kudva, R., Muller, M., and Daley, D.O. (2014). YfgM is an ancillary subunit of the SecYEG translocon in Escherichia coli. J. Biol. Chem. *289*, 19089–19097.

Green, E.R., and Mecsas, J. (2016). Bacterial Secretion Systems: An Overview. Microbiol Spectr *4*.

Gu, Y., Li, H., Dong, H., Zeng, Y., Zhang, Z., Paterson, N.G., Stansfeld, P.J., Wang, Z., Zhang, Y., Wang, W., et al. (2016). Structural basis of outer membrane protein insertion by the BAM complex. Nature *531*, 64–69.

Humes, J.R., Schiffrin, B., Calabrese, A.N., Higgins, A.J., Westhead, D.R., Brockwell, D.J., and Radford, S.E. (2019). The Role of SurA PPIase Domains in Preventing Aggregation of the Outer-Membrane Proteins tOmpA and OmpT. J. Mol. Biol.

Iadanza, M.G., Higgins, A.J., Schiffrin, B., Calabrese, A.N., Brockwell, D.J., Ashcroft, A.E., Radford, S.E., and Ranson, N.A. (2016). Lateral opening in the intact β-barrel assembly machinery captured by cryo-EM. Nature Communications *7*, 12865.

Josefsson, L.G., and Randall, L.L. (1981). Different exported proteins in E. coli show differences in the temporal mode of processing in vivo. Cell *25*, 151–157.

Kastner, B., Fischer, N., Golas, M.M., Sander, B., Dube, P., Boehringer, D., Hartmuth, K., Deckert, J., Hauer, F., Wolf, E., et al. (2008). GraFix: sample preparation for single-particle electron cryomicroscopy. Nat. Methods *5*, 53–55.

Kimanius, D., Forsberg, B.O., Scheres, S.H., and Lindahl, E. (2016). Accelerated cryo-EM structure determination with parallelisation using GPUs in RELION-2. eLife *5*.

Komar, J., Alvira, S., Schulze, R.J., Martin, R., Lycklama A Nijeholt, J.A., Lee, S.C., Dafforn, T.R., Deckers-Hebestreit, G., Berger, I., Schaffitzel, C., et al. (2016). Membrane protein insertion and assembly by the bacterial holo-translocon SecYEG-SecDF-YajC-YidC. Biochem. J. *473*, 3341–3354.

Konovalova, A., Kahne, D.E., and Silhavy, T.J. (2017). Outer Membrane Biogenesis. Annu. Rev. Microbiol. *71*, 539–556.

la Rosa-Trevín, de, J.M., Otón, J., Marabini, R., Zaldívar, A., Vargas, J., Carazo, J.M., and Sorzano, C.O.S. (2013). Xmipp 3.0: an improved software suite for image processing in electron microscopy. J. Struct. Biol. *184*, 321–328.

la Rosa-Trevín, de, J.M., Quintana, A., Del Cano, L., Zaldívar, A., Foche, I., Gutiérrez, J., Gómez-Blanco, J., Burguet-Castell, J., Cuenca-Alba, J., Abrishami, V., et al. (2016). Scipion: A software framework toward integration, reproducibility and validation in 3D electron microscopy. J. Struct. Biol. *195*, 93–99.

Lill, R., Cunningham, K., Brundage, L.A., Ito, K., Oliver, D., and Wickner, W. (1989). SecA protein hydrolyzes ATP and is an essential component of the protein translocation ATPase of Escherichia coli. Embo J. *8*, 961–966.

Lotz, M., Haase, W., Kühlbrandt, W., and Collinson, I. (2008). Projection structure of yidC: a conserved mediator of membrane protein assembly. J. Mol. Biol. *375*, 901–907.

McMorran, L.M., Bartlett, A.I., Huysmans, G.H.M., Radford, S.E., and Brockwell, D.J. (2013). Dissecting the effects of periplasmic chaperones on the in vitro folding of the outer membrane

protein PagP. J. Mol. Biol. *425*, 3178–3191.

Miroux, B., and Walker, J.E. (1996). Over-production of proteins in Escherichia coli: mutant hosts that allow synthesis of some membrane proteins and globular proteins at high levels. J. Mol. Biol. *260*, 289–298.

Nishiyama, K., Hanada, M., and Tokuda, H. (1994). Disruption of the gene encoding p12 (SecG) reveals the direct involvement and important function of SecG in the protein translocation of Escherichia coli at low temperature. Embo J. *13*, 3272–3277.

Ott, C., Dorsch, E., Fraunholz, M., Straub, S., and Kozjak-Pavlovic, V. (2015). Detailed analysis of the human mitochondrial contact site complex indicate a hierarchy of subunits. PLoS ONE *10*, e0120213.

Pettersen, E.F., Goddard, T.D., Huang, C.C., Couch, G.S., Greenblatt, D.M., Meng, E.C., and Ferrin, T.E. (2004). UCSF Chimera--a visualization system for exploratory research and analysis. J Comput Chem *25*, 1605–1612.

Rampelt, H., Bohnert, M., Zerbes, R.M., Horvath, S.E., Warscheid, B., Pfanner, N., and van der Laan, M. (2017). Mic10, a Core Subunit of the Mitochondrial Contact Site and Cristae Organizing System, Interacts with the Dimeric F1Fo-ATP Synthase. J. Mol. Biol. *429*, 1162–1170.

Rassam, P., Copeland, N.A., Birkholz, O., Tóth, C., Chavent, M., Duncan, A.L., Cross, S.J., Housden, N.G., Kaminska, R., Seger, U., et al. (2015). Supramolecular assemblies underpin turnover of outer membrane proteins in bacteria. Nature *523*, 333–336.

Rassam, P., Long, K.R., Kaminska, R., Williams, D.J., Papadakos, G., Baumann, C.G., and Kleanthous, C. (2018). Intermembrane crosstalk drives inner-membrane protein organization in Escherichia coli. Nature Communications *9*, 1082.

Ricci, D.P., and Silhavy, T.J. (2019). Outer Membrane Protein Insertion by the β-barrel Assembly Machine. EcoSal Plus *8*.

Roman-Hernandez, G., Peterson, J.H., and Bernstein, H.D. (2014). Reconstitution of bacterial autotransporter assembly using purified components. eLife *3*, e04234.

Rosenthal, P.B., and Henderson, R. (2003). Optimal determination of particle orientation, absolute hand, and contrast loss in single-particle electron cryomicroscopy. J. Mol. Biol. *333*, 721–745.

Scheres, S.H.W. (2012a). RELION: implementation of a Bayesian approach to cryo-EM structure determination. J. Struct. Biol. *180*, 519–530.

Scheres, S.H.W. (2012b). A Bayesian view on cryo-EM structure determination. J. Mol. Biol. *415*, 406–418.

Scheres, S.H.W., and Chen, S. (2012). Prevention of overfitting in cryo-EM structure

determination. Nat. Methods *9*, 853–854.

Schiebel, E., Driessen, A.J., Hartl, F.U., and Wickner, W. (1991). Delta mu H+ and ATP function at different steps of the catalytic cycle of preprotein translocase. Cell *64*, 927–939.

Schiffrin, B., Calabrese, A.N., Higgins, A.J., Humes, J.R., Ashcroft, A.E., Kalli, A.C., Brockwell, D.J., and Radford, S.E. (2017). Effects of Periplasmic Chaperones and Membrane Thickness on BamA-Catalyzed Outer-Membrane Protein Folding. J. Mol. Biol. *429*, 3776–3792.

Schulze, R.J., Komar, J., Botte, M., Allen, W.J., Whitehouse, S., Gold, V.A.M., Lycklama A Nijeholt, J.A., Huard, K., Berger, I., Schaffitzel, C., et al. (2014). Membrane protein insertion and proton-motive-force-dependent secretion through the bacterial holo-translocon SecYEG-SecDF-YajC-YidC. Proc. Natl. Acad. Sci. U.S.a. *111*, 4844–4849.

Selkrig, J., Mosbahi, K., Webb, C.T., Belousoff, M.J., Perry, A.J., Wells, T.J., Morris, F., Leyton, D.L., Totsika, M., Phan, M.-D., et al. (2012). Discovery of an archetypal protein transport system in bacterial outer membranes. Nat. Struct. Mol. Biol. *19*, 506–10–S1.

Sklar, J.G., Wu, T., Kahne, D., and Silhavy, T.J. (2007). Defining the roles of the periplasmic chaperones SurA, Skp, and DegP in Escherichia coli. Genes Dev. *21*, 2473–2484.

Sorzano, C.O.S., Bilbao-Castro, J.R., Shkolnisky, Y., Alcorlo, M., Melero, R., Caffarena-Fernández, G., Li, M., Xu, G., Marabini, R., and Carazo, J.M. (2010). A clustering approach to multireference alignment of single-particle projections in electron microscopy. J. Struct. Biol. *171*, 197–206.

Tang, G., Peng, L., Baldwin, P.R., Mann, D.S., Jiang, W., Rees, I., and Ludtke, S.J. (2007). EMAN2: an extensible image processing suite for electron microscopy. J. Struct. Biol. *157*, 38–46.

Thonghin, N., Kargas, V., Clews, J., and Ford, R.C. (2018). Cryo-electron microscopy of membrane proteins. Methods *147*, 176–186.

Tsukazaki, T., Mori, H., Echizen, Y., Ishitani, R., Fukai, S., Tanaka, T., Perederina, A., Vassylyev, D.G., Kohno, T., Maturana, A.D., et al. (2011). Structure and function of a membrane component SecDF that enhances protein export. Nature *474*, 235–238.

Vahedi-Faridi, A., Jastrzebska, B., Palczewski, K., and Engel, A. (2013). 3D imaging and quantitative analysis of small solubilized membrane proteins and their complexes by transmission electron microscopy. Microscopy (Oxf) *62*, 95–107.

Van den Berg, B., Clemons, W.M., Collinson, I., Modis, Y., Hartmann, E., Harrison, S.C., and Rapoport, T.A. (2004). X-ray structure of a protein-conducting channel. Nature *427*, 36–44.

Voulhoux, R., Bos, M.P., Geurtsen, J., Mols, M., and Tommassen, J. (2003). Role of a highly conserved bacterial protein in outer membrane protein assembly. Science *299*, 262–265.

Wang, Z., Fan, G., Hryc, C.F., Blaza, J.N., Serysheva, I.I., Schmid, M.F., Chiu, W., Luisi, B.F.,

and Du, D. (2017). An allosteric transport mechanism for the AcrAB-TolC multidrug efflux pump. eLife *6*.

Wu, T., Malinverni, J., Ruiz, N., Kim, S., Silhavy, T.J., and Kahne, D. (2005). Identification of a multicomponent complex required for outer membrane biogenesis in Escherichia coli. Cell *121*, 235–245.

Zuber, B., Chami, M., Houssin, C., Dubochet, J., Griffiths, G., and Daffé, M. (2008). Direct visualization of the outer membrane of mycobacteria and corynebacteria in their native state. J. Bacteriol. *190*, 5672–5680.

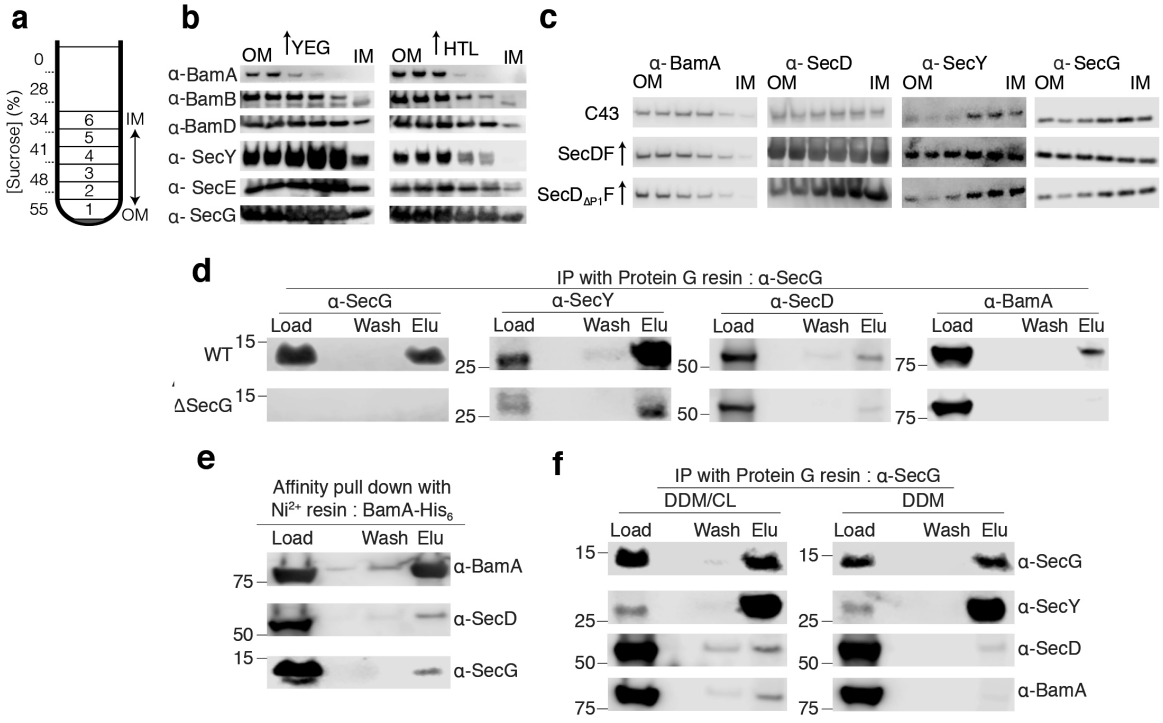

Figure. 1: Identification of interactions between HTL and BAM

a, Schematic representation of sucrose gradient centrifugation tube for fractionation of *E. coli* total membranes. Numbers 1-6 indicate the fractions taken for western blots shown in **b** and **c**.

b, c, Western blots of sucrose gradient fractions of *E. coli* C43 total membranes from cells over-producing SecYEG or HTL (**b**); and from the *E. coli* C43 with no over-expression, and those over-producing either SecDF or SecD$_{\Delta P1}$F (lacking the periplasmic domain 1 – P1 of SecD) (**c**).

d, e, f, Co-immuno-precipitations (co-IP) of SecG, SecY, SecD and BamA – pulling with the SecG antibody (**d**); affinity pull-down of recombinant BamA-His$_6$, SecD and SecG by nickel chelation (**e**); and cardiolipin (CL) dependence of HTL-BAM interaction demonstrated by co-IP as described in **d** (**f**). Pull-downs were conducted with solubilised crude membrane extracts from *E. coli* C43, a strain lacking SecG (Δ*secG*), and C43 over-producing BAM.

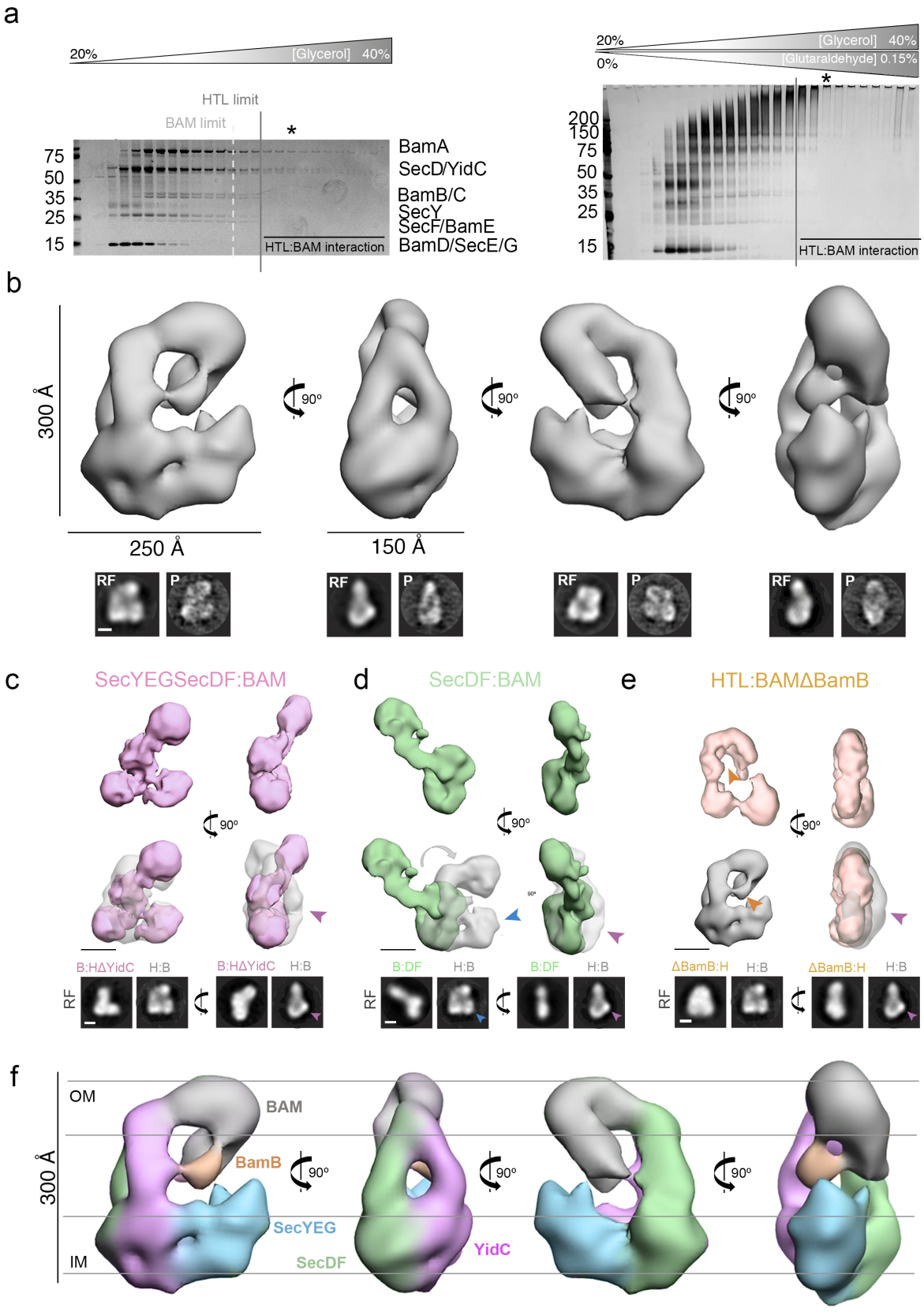

Figure. 2: Isolation and 3D characterization of HTL-BAM super-complex in detergent.

a, Silver stained SDS-PAGE analysis of HTL-BAM fractionated by glycerol density gradient centrifugation (left), and of HTL-BAM GraFix experiment (right). BAM limit and HTL limit show the furthest fraction to which the individual complexes migrate alone (taken from Extended figure 1a). Asterisk shows the fraction chosen for EM and image processing.

b, Top, four orthogonal views of the HTL-BAM complex 3D reconstruction (37.2 Å resolution). Bottom, reference-free (RF) class averages and projections (P) of the final model, shown in the same orientations as at the top. Scale bar, 100 Å. See Table S2 for image processing details.

For **c, d** and **e,** top panel shows frontal and lateral views of 3D reconstructions, middle panel shows the top panel superimposed with HTL-BAM (transparent grey) from **b,** and bottom shows a comparison of frontal and lateral reference-free (RF) class averages of HTL-BAM with the corresponding structure. Scale bar, 100 Å. See Table S2 for image processing details.

c, SecYEG-SecDF-BAM complex 3D reconstruction (36.7 Å resolution, pink). Pink arrow indicates the extra mass in HTL-BAM (grey transparent) corresponding to YidC.

d, SecDF-BAM complex 3D reconstruction (39.4 Å resolution, green). Pink arrow points to the extra mass corresponding to YidC. Blue arrow points to the extra mass corresponding to SecYEG. Grey arrow illustrated the dislocation of BAM apparent in the SecDF-BAM structure relative to HTL-BAM (see also Extended Data 4).

e, HTL-BAM(ΔBamB) complex 3D reconstruction (33.6 Å resolution, orange). Pink arrow points to the extra mass corresponding to YidC. Orange arrow points to the extra mass corresponding to BamB.

f, Coloured map of HTL-BAM complex components in four representative orthogonal views.

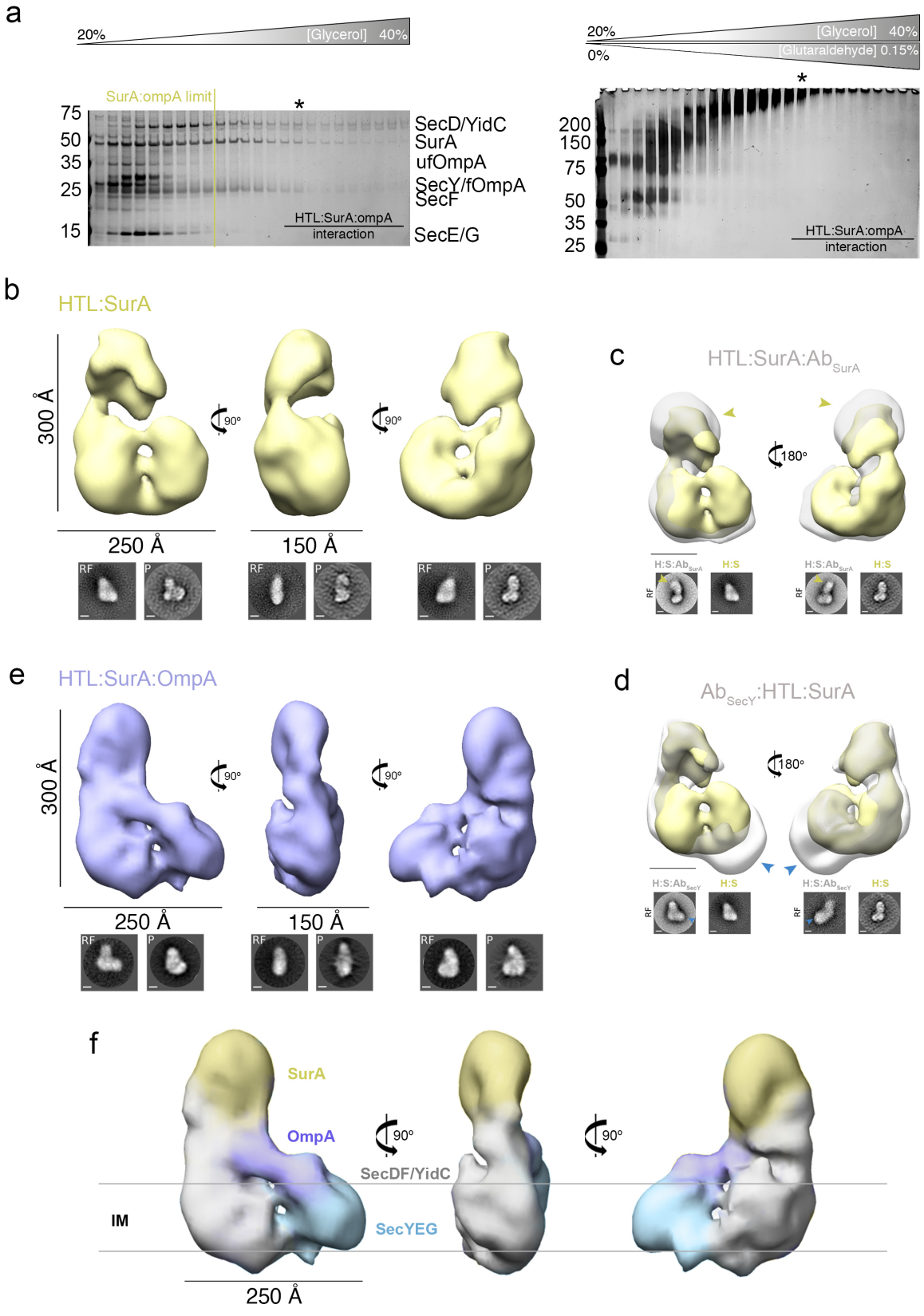

Figure. 3: Isolation and 3D characterization of the HTL:SurA and HTL:SurA-OmpA complexes.

a, Example silver-stained SDS-PAGE analysis of HTL:SurA-OmpA fractionated by glycerol density gradient centrifugation (left), and the same for HTL:SurA-OmpA GraFix experiment (right). Asterisk shows the fraction chosen for EM and image processing. SurA limit shows the furthest fraction to which SurA migrates alone (taken from Extended figure 6a).

For **b**, **c, d,** and **e,** top panel shows views of 3D reconstructions, and bottom show reference-free (RF) class averages and projections (P) of the final model, shown in the same orientations as the top. Scale bars are 100 Å, unless otherwise stated. See Table S2 for image processing details.

b, Orthogonal views of the HTL-SurA complex 3D reconstruction (41.9 Å resolution).

c, Orthogonal views of the HTL-SurA complex (yellow) superimposed on the immuno-complex HTL-SurA:Ab_{SurA} complex (grey). The antibody (yellow arrows) is shown bound to the mass assigned to SurA.

d, Frontal and back views of the HTL-SurA complex (yellow) superimposed on the inmunocomplex Ab_{SecY}:HTL-SurA complex (grey). The antibody (blue arrows) is shown bound to the mass assigned to SecY.

e, Frontal, lateral and back views of the HTL-SurA:OmpA complex 3D reconstruction (37.5 Å resolution).

f, Coloured map of the HTL-SurA-ompA complex components in the three representative orthogonal views.

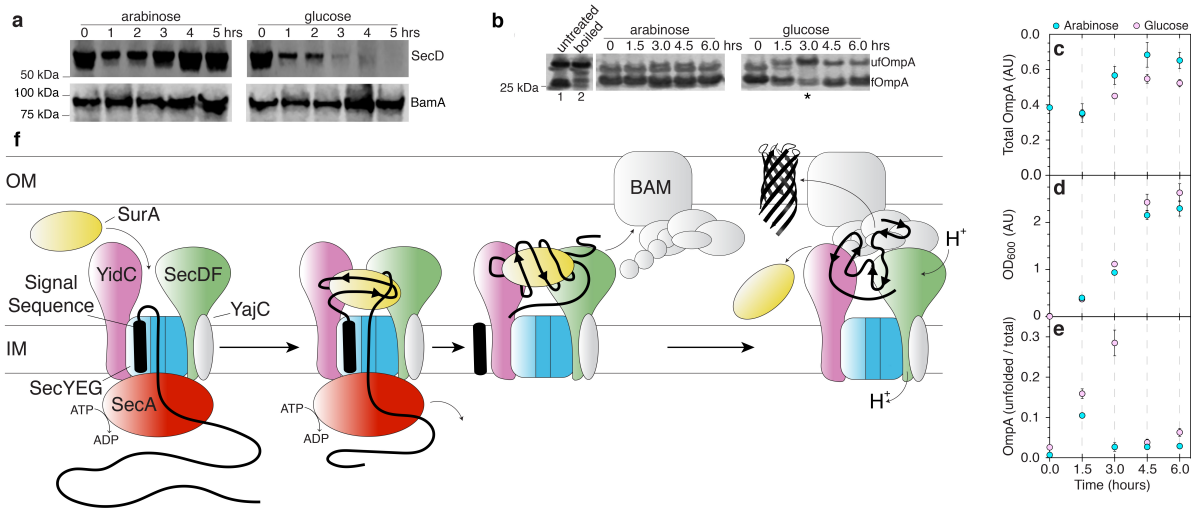

Figure 4: Deficiency of OmpA insertion when SecDF-YajC is downregulated

a, Western blot illustrating depletion of SecD and unaltered levels of BamA in *E. coli* JP325 whole cells when grown in the presence of arabinose or glucose.

b, Western blot illustrating periplasmic unfolded outer membrane protein A (OmpA) during SecDF-YajC depletion (glucose), compared to basal levels (arabinose). Also shown are control lanes containing *E. coli* whole cells with over-produced, mainly 'folded' OmpA (1, fOmpA, bottom band) and the same sample, but boiled, to produce 'unfolded' OmpA (2, ufOmpA, top band).

c, e, Analysis of western blots such as that from Figure 4a showing the ratio of ufOmpA to fOmpA in the periplasmic fraction (**c**) and the total periplasmic OmpA (**d**) during SecDF-YajC depletion. Error bars represent SEM for n=4, and those error bars smaller than data points are not shown.

d, Growth curve of *E. coli* JP325 in the presence of arabinose (basal SecDF-YajC levels) or glucose (depletion of SecDF-YajC). Error bars represent SEM for n=3, and those error bars smaller than data points are not shown.

f, Schematic model of OMP transfer through HTL-SurA and HTL-BAM. The scheme depicts how the Sec-translocon operates during SecA driven post-translational transport of a precursor outer membrane protein (OMP), and how the interaction with the BAM could facilitate energy coupling and efficient transport of large quantities of protein to the OM. The precise coordination with the periplasmic chaperones (*e.g.* SurA) is unclear, though they presumably contact the Sec-machinery (this study) and BAM(Sklar et al., 2007). Note the prospect of coupling the energy available in the trans-membrane proton-motive-force (PMF) *via* SecD (lower right), and from ATP by potential re-engagement of SecA.

SUPPLEMENTARY MATERIAL:

Trans-membrane association of the Sec and BAM complexes for bacterial outer-membrane biogenesis

Sara Alvira[1*], Daniel W. Watkins[1*], Lucy Troman[1], James Lorriman[1], Bertram Daum[2], Vicki A.M. Gold[2] and Ian Collinson[1†]

[1], School of Biochemistry, University of Bristol, BS8 1TD, United Kingdom

[2], Living Systems Institute, Stocker Road, Exeter, Devon EX4 4QD, United Kingdom

[*], these authors contributed equally to this work

[†], corresponding author: ian.collinson@bristol.ac.uk

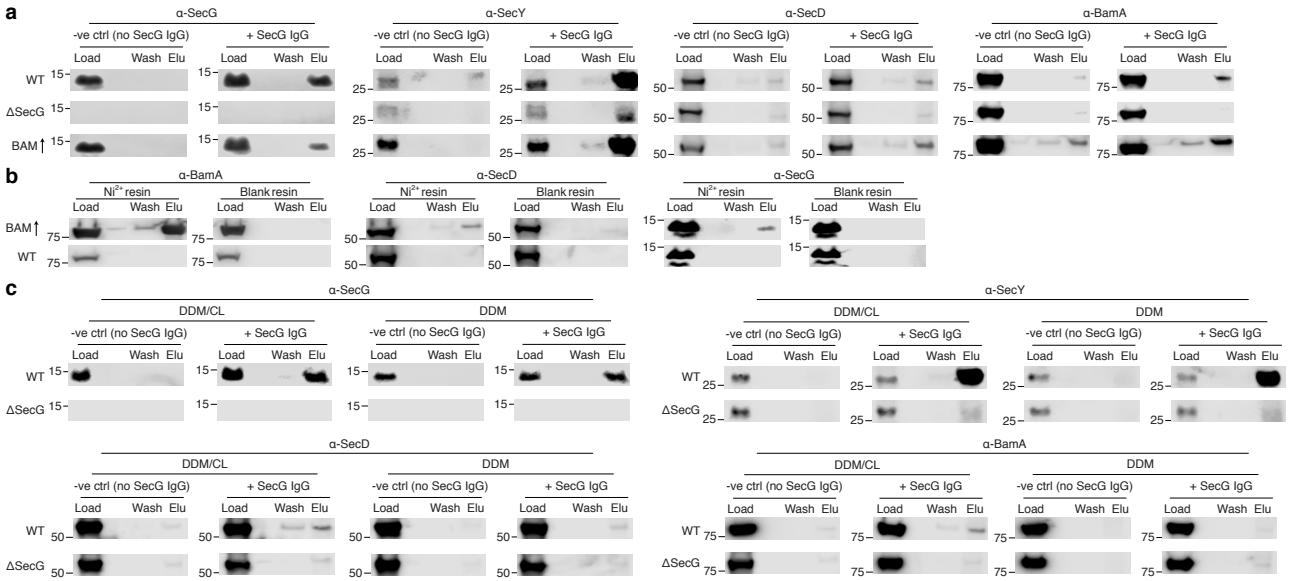

Fig. S1.

Identification of interactions between HTL and BAM

a, Co-immunoprecipitation (co-IP) of SecG, SecY, SecD and BamA when pulling on a SecG antibody. Negative controls are shown where SecG antibody was not included in the pull downs.

b, Affinity pull down of recombinant BamA-His_6, SecD and SecG when pulling on the His tag of BamA with nickel resin. Controls with non-overproduced BamA-His_6 are shown.

c, Cardiolipin dependence of the HTL-BAM interaction demonstrated in **a**. Pull downs were performed in the presence of detergent (DDM) or a DDM supplemented with cardiolipin (CL).

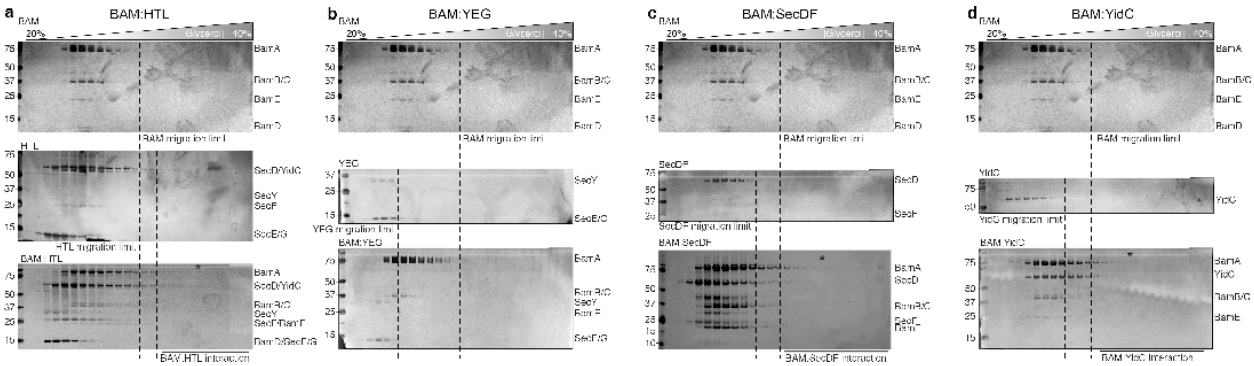

Fig. S2.

Glycerol centrifugation gradients of HTL and BAM components.

a, b, c, d, Silver-stained SDS-PAGE gels of glycerol centrifugation gradients are shown, with increasingly massive complexes appearing in fractions of higher percentage glycerol. For each letter, the glycerol centrifugation gradient of BAM alone is shown (top). The middle gel represents HTL or a HTL component (labelled on the top left of the gel). The bottom gel represents the experiment where BAM was mixed with the corresponding HTL component. Dashed lines represent the fraction of furthest migration, as determined in the top two gels.

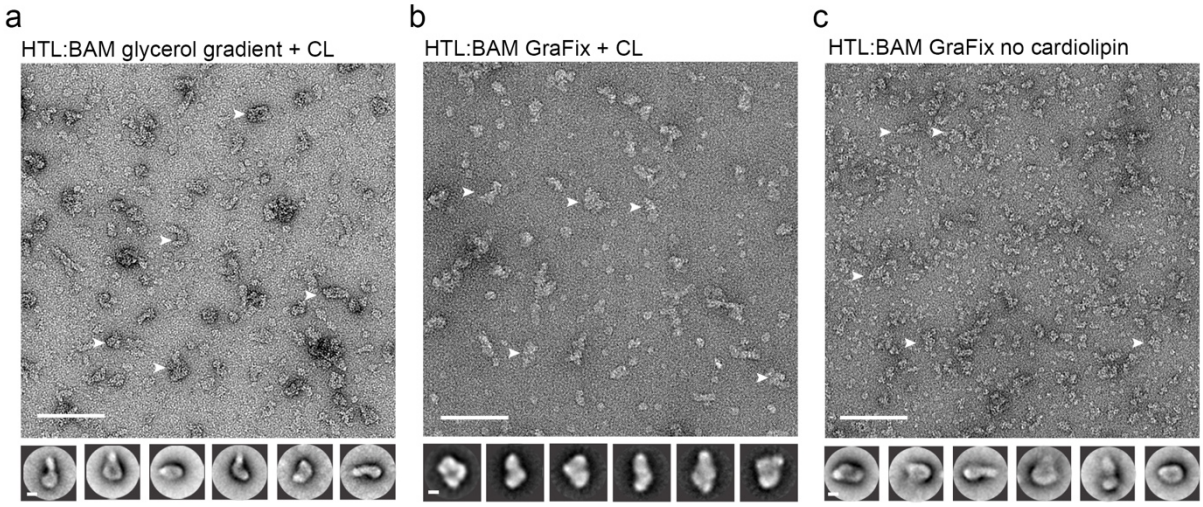

Fig. S3.

EM of HTL:BAM complex.

a, b, c, Electron micrographs of HTL-BAM complexes in different conditions. Bottom, reference-free (RF) class averages of the biggest populations found in the micrographs. Micrograph scale bar, 1000 Å. RF scale bar, 100 Å. White arrows indicate representative HTL:BAM complexes used for image processing.

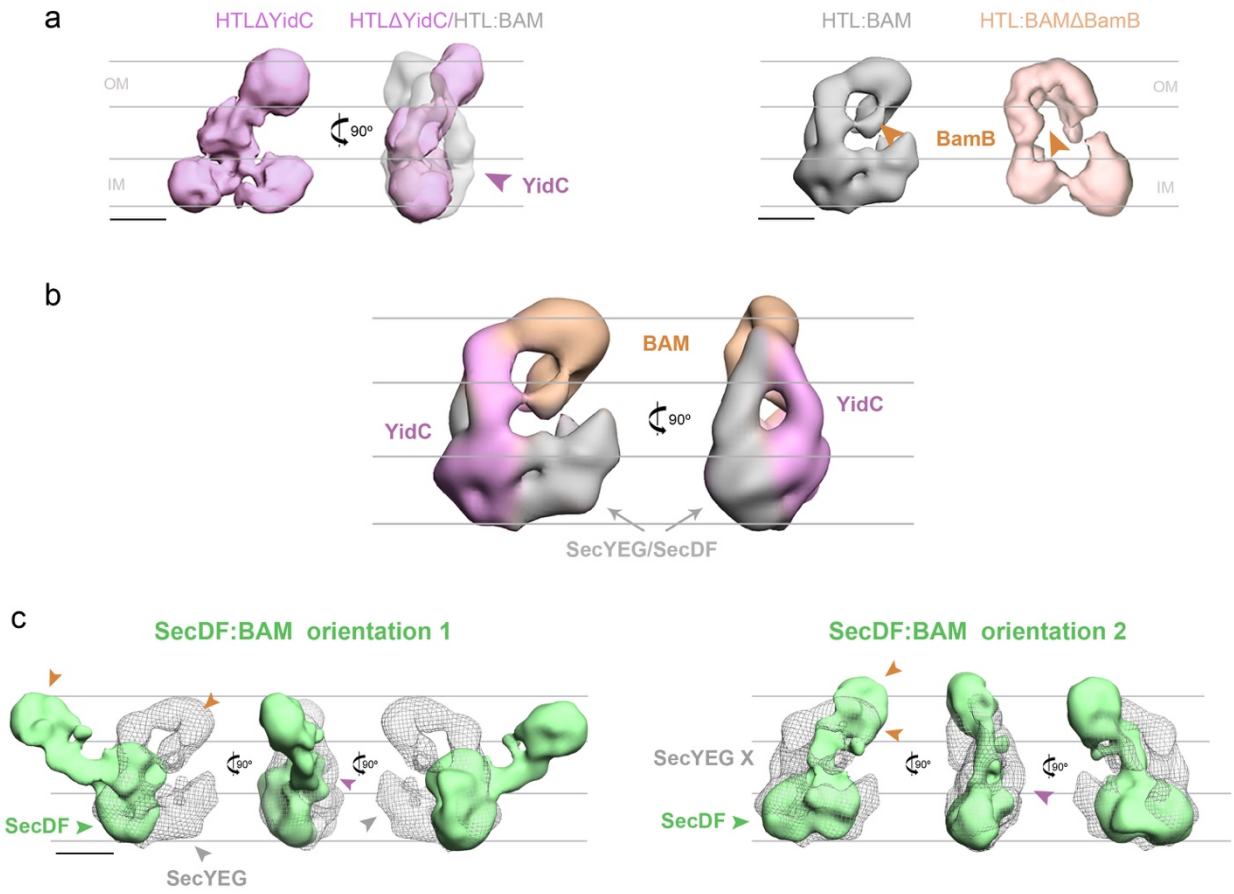

Fig. S4.

Assignation of the SecDF-BAM structure orientation

a, Left, assignation of YidC extracted from Figure 2c. Pink arrow, location of YidC. Right, assignation of BamB extracted from Figure 2e. Orange arrow, location of BamB

b, Frontal and lateral view of the HTL-BAM complex. Grey unassigned extra mass correspond to SecYEG and SecDF

c, Two different orientations of the SecDF-BAM complex according with comparision with the HTL:BAM complex (grey mesh). Left, orientation chosen at Figure 2d. SecDF is placed as same position of SecYEG-SecDF-BAM complex (a, pink), leaving the unsigned mass (grey label) at the IM for SecYEG and showing a movement of the BAM machinery (orange arrows). Right, second orientation choice (non-correct). BAM (orange arrows) is placed at the same relative position as HTL-BAM. SecDF (grey arrow) is fully located within the IM and the unsigned mass at the periplasmic space would correspond with SecYEG (grey cross).

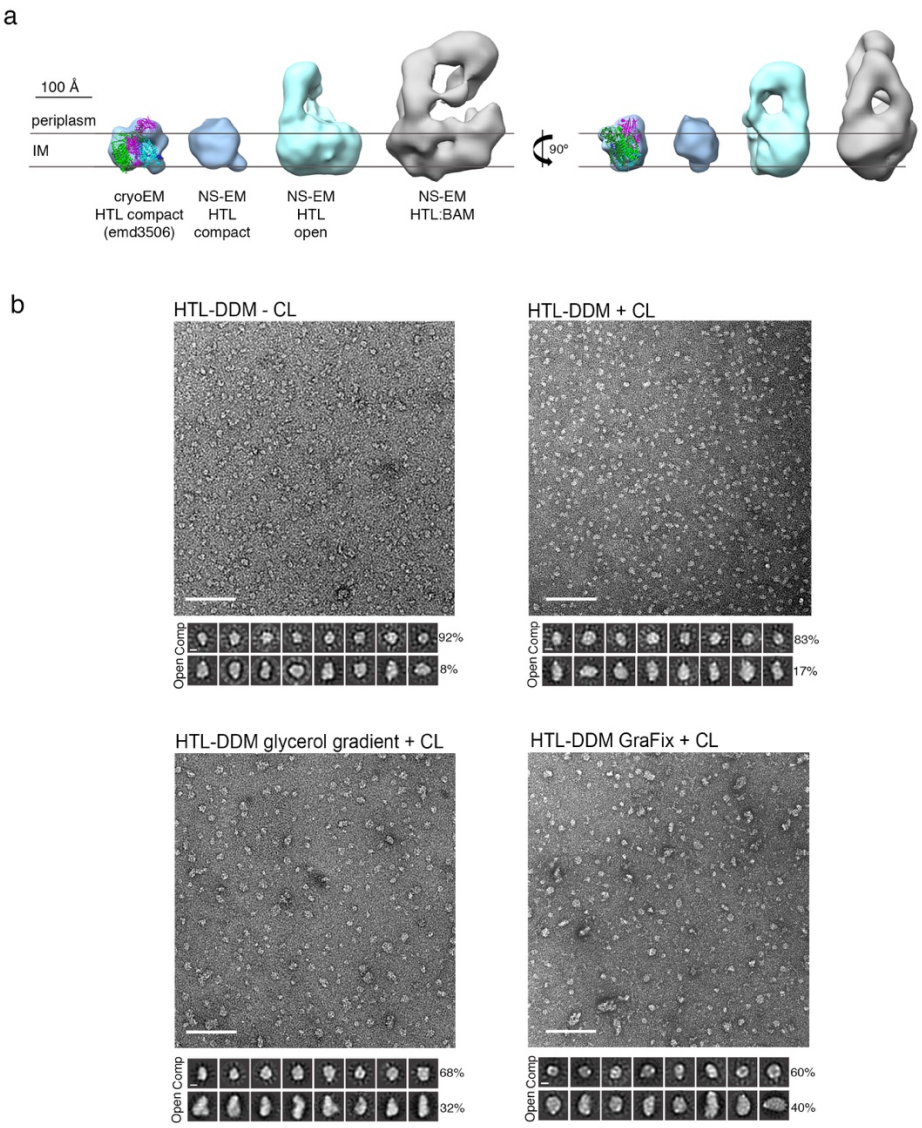

Fig. S5.
NS-EM of the HTL complex.

a, Size comparison of the 3D structures at their frontal and lateral views with the compact published cryo-HTL (emd3506), our compact NS-HTL structure, our open NS-HTL structure and the NS HTL:BAM complex.

b, Top, EM field of HTL in different conditions. Bottom, reference-free (RF) class averages of the compact (Comp) and open populations found in the micrographs. Percentage of the populations are indicated on the right RF images. Micrograph scale bar, 1000 Å. RF scale bar, 100 Å.

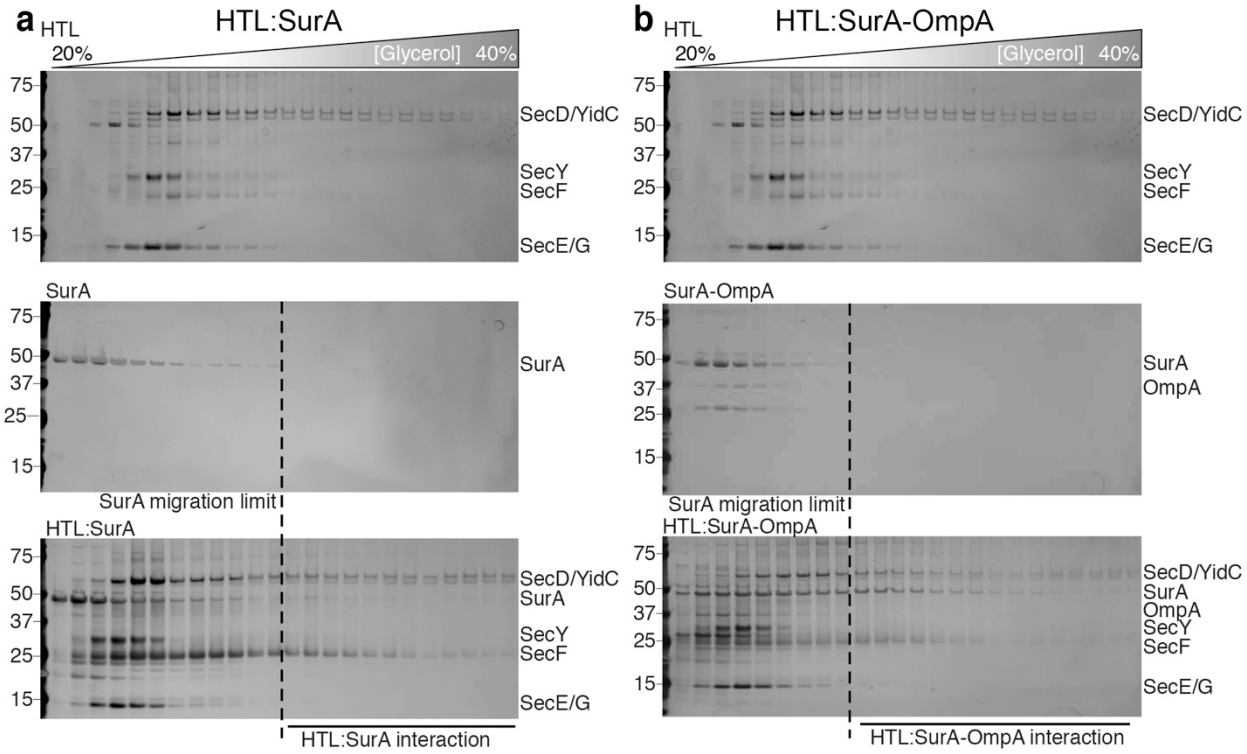

Fig. S6.
Glycerol centrifugation gradients of HTL-SurA and HTL-SurA-ompA complexes.

For **a** and **b**, the experiment was conducted as in **Fig. S2.**

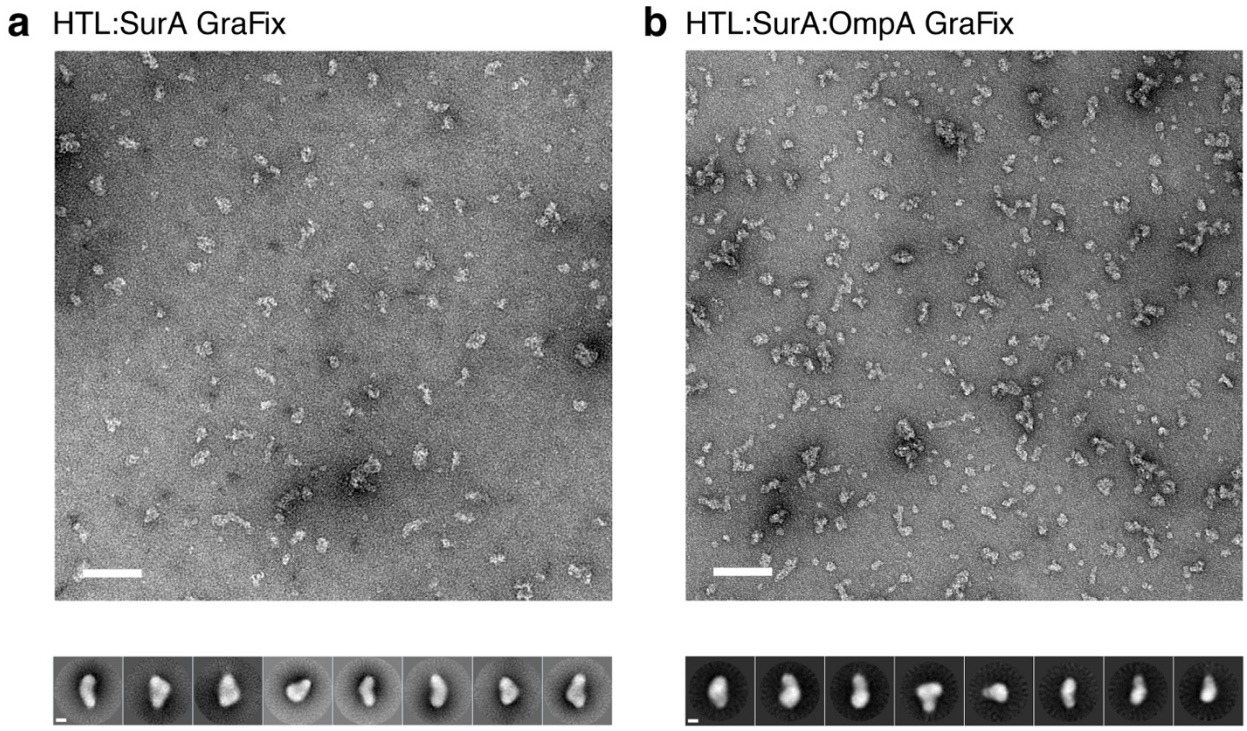

Fig. S7.

EM of HTL-SurA and HTL-SurA-OmpA complexes.

Top: EM fields of HTL:SurA (**a**) and HTL:SuraA:OmpA (**b**) prepared using GraFix. Bottom, reference-free (RF) class averages of the biggest populations from corresponding micrographs. Micrograph scale bar, 1000 Å. RF scale bar, 100 Å

Table 1: Mass spectometry analysis of the GraFix fractions for image processing

Sample		Accession	Description	Score	Coverage	rotal	Peptid	# PSMs	Area
BAM:HTL detergent		B7UJN1	Protein translocase subunit SecD OS=Escherichia coli O127:H6 (strain E2348/69 / EPEC) OX=574521 GN=secD PE=3 SV=1 - [B7UJN1_ECO27]	1166.56	53.01	1	35	403	4.609E+8
		B7UIM2	Outer membrane protein assembly factor BamA OS=Escherichia coli O127:H6 (strain E2348/69 / EPEC) OX=574521 GN=bamA PE=3 SV=1 - [BAMA_ECO27]	683.99	60.74	1	46	257	7.500E+7
		B7UGM7	Outer membrane protein assembly factor BamC OS=Escherichia coli O127:H6 (strain E2348/69 / EPEC) OX=574521 GN=nlpB PE=3 SV=1 - [B7UGM7_ECO27]	404.02	55.81	1	14	119	3.642E+7
		B7UJN2	Protein-export membrane protein SecF OS=Escherichia coli O127:H6 (strain E2348/69 / EPEC) OX=574521 GN=secF PE=3 SV=1 - [B7UJN2_ECO27]	249.64	27.55	1	7	74	2.772E+7
		B7UMH2	Membrane protein insertase YidC OS=Escherichia coli O127:H6 (strain E2348/69 / EPEC) OX=574521 GN=yidC PE=3 SV=1 - [YIDC_ECO27]	181.06	36.31	1	13	64	3.983E+7
		B7UH30	Outer membrane protein assembly factor BamD OS=Escherichia coli O127:H6 (strain E2348/69 / EPEC) OX=574521 GN=yfiO PE=3 SV=1 - [B7UH30_ECO27]	173.40	66.12	1	15	76	3.235E+7
		B7UGV8	Outer membrane protein assembly factor BamB OS=Escherichia coli O127:H6 (strain E2348/69 / EPEC) OX=574521 GN=yfgL PE=3 SV=1 - [B7UGV8_ECO27]	129.35	34.44	1	11	45	3.143E+7
		B7UK24	Protein translocase subunit SecY OS=Escherichia coli O127:H6 (strain E2348/69 / EPEC) OX=574521 GN=secY PE=3 SV=1 - [B7UK24_ECO27]	36.43	15.58	1	5	14	3.454E+6
SurA:HTL detergent		B7UJN1	Protein translocase subunit SecD OS=Escherichia coli O127:H6 (strain E2348/69 / EPEC) OX=574521 GN=secD PE=3 SV=1 - [B7UJN1_ECO27]	1098.08	50.57	1	33	393	6.386E+8
		B7UMH2	Membrane protein insertase YidC OS=Escherichia coli O127:H6 (strain E2348/69 / EPEC) OX=574521 GN=yidC PE=3 SV=1 - [YIDC_ECO27]	266.32	32.66	1	13	98	1.235E+8
		B7UJN2	Protein-export membrane protein SecF OS=Escherichia coli O127:H6 (strain E2348/69 / EPEC) OX=574521 GN=secF PE=3 SV=1 - [B7UJN2_ECO27]	236.81	18.27	1	5	70	4.934E+7
		B7UIA1	Chaperone SurA OS=Escherichia coli O127:H6 (strain E2348/69 / EPEC) OX=574521 GN=surA PE=3 SV=1 - [B7UIA1_ECO27]	49.97	23.60	1	10	23	3.360E+6
		B7UK24	Protein translocase subunit SecY OS=Escherichia coli O127:H6 (strain E2348/69 / EPEC) OX=574521 GN=secY PE=3 SV=1 - [B7UK24_ECO27]	7.01	4.51	1	3	4	1.931E+6

Table S1.

Mass spectroscopy analysis.

Analysis composition by MS of the complexes HTL-BAM in detergent and HTL-SurA. The SDS-gel bands corresponding to the GraFix fractions used for EM processing were cropped and analysed by MS.

Table 1: Image processing details

Complex	Initial particles	High quality particles	Final 3D volume	Resolution
HTL-DDM	100754	74070	-	-
HTL-DDM+CL	22869	18674	-	-
HTLafter gradient+CL	21735	18434	-	-
HTLafter gradient+gluta.+CL	101142	90432	9656 (compact conformation)	26,56A
			1569 (extended conformation)	39,54 A
HTL:BAM Δgluta	29336	12460	-	-
HTL:BAM grafix	65381	28646	5122	37,2A
HTL:BAM grafix ΔCL	14530	11406	-	-
SecDF:BAM	22642	11987	5430	39,4A
HTLΔYidC:BAM	16008	8612	4943	36,7A
HTL:BAMΔB	31561	11484	3919	33,65A
SurA:HTL	24252	18696	2290	41,88 A
SurA:HTL:Ab$_{SecY}$	15819	9510	4431	47,06 A
Ab$_{SurA}$:SurA:HTL	14246	3882	730	56,67 A
SurA:HTL:OmpA	35546	33485	11699	37,50 A

Table S2.

Particle composition in the 3D image processing.

Summary of the particles selected and processed for the different image analysis of the complexes described in this study. Dash indicates the processing only reached an analysis at 2D level.